Solid State Communications 249 (2017) 1–6

Contents lists available at ScienceDirect

Solid State Communications

journal homepage: www.elsevier.com/locate/ssc

Communication

Substrate induced anomalous electrostatic and photoluminescence propeties of monolayer MoS_2 edges

Song Hao[a,b], Bingchu Yang[a,b,*], Jingye Yuan[a], Yongli Gao[a,b,c]

[a] Institute of Super Microstructure and Ultrafast Process in Advanced Materials, College of Physics and Electronics, Central South University, 605 South Lushan Road, Changsha 410012, PR China

[b] Hunan Key Laboratory for Super-microstructure and Ultrafast Process, Central South University, 932 South Lushan Road, Changsha 410012, PR China

[c] Department of Physics and Astronomy, University of Rochester, Rochester, NY 14534, USA

ARTICLE INFO

Keywords:
Molybdenum disulfide
Substrate effects
Charge transfer
Doping level
Thermal strain
Photoluminescence spectroscopy

ABSTRACT

Monolayer MoS_2 is an emerging two-dimensional semiconductor with wide-ranging potential applications in the next generation electronic and optoelectronic devices. Understanding the influences of the supporting substrates on the physical properties of grown MoS_2 is an important step toward its applications. Here we synthesized two typical rhomboid shaped MoS_2 on MoO_2 and triangle shaped MoS_2 on SiO_2/Si substrates and characterized them by multiple means of X-Ray Photoemission Spectroscopy, Atomic Force Microscopy, Electrostatic Force Microscopy, Raman and Photoluminescence techniques. We found that triangle shaped MoS_2 exhibits different core level spectra compared with rhomboid shaped MoS_2, attributed to dissimilar charge transfer with the underlying SiO_2 substrate. Interestingly, the triangle shaped MoS_2 single crystals exhibit distinct electrostatic and photoluminescence properties at center and edges. The underlying mechanism is proposed that partial decoupling of MoS_2 at edges from SiO_2 substrate induces different doping level and strain effects, resulting in anomalous physical properties at edges. The results reported here demonstrate that doping and strain effects induced by substrates have a significant influence on physical properties of monolayer triangle shaped MoS_2 , which can be generally applicable to other transition metal dichalcogenides materials.

1. Introduction

Graphene is one of the most popular two-dimensional (2D) materials, due to its intriguing physical properties and enormous potential applications, such as condensed matter physics, electronics, and energy storage and conversion [1]. However, its gapless nature slows the development in electronic and optoelectronic devices applications. Following the boom of graphene, transition metal dichalcogenides (TMDCs) materials have emerged as an important layered crystals, exhibiting intrinsic semiconducting, metallic and even superconducting behaviors [2–4]. Generally, TMDCs materials have the formula MX_2, where M represents a transition metal from groups IV-VI (e.g. Mo, W, Ti, or Nb), while X is a chalcogen atom (S, Se, or Te). More than 40 types of TMDCs occur depending on the combination of chalcogen and metal atoms [2]. Among them, MoS_2 is a representative one with good chemical stability, excellent optical and electrical properties. In the bulk form, the semiconducting MoS_2 has an indirect bandgap of ~1.2 eV while monolayer MoS_2 has a direct bandgap of ~1.8 eV [5]. Such changes in the bandgap when reducing the thickness of a MoS_2 crystals have a considerable implications for the development of novel devices. For example, monolayer MoS_2 has been fabricated to many prototype devices with advanced functionalities, such as field-effect transistors (FETs), chemical sensors, photonic detectors, and integrated circuit [6–8].

Exploring an approach to synthesize scalable and high-crystalline monolayer MoS_2 is necessary to realize those enormous advantages. The chemical vapor deposition (CVD) method, a powerful way to large-scale graphene, allows the growth of single-crystalline MoS_2 microflakes directly on arbitrary substrates [9–11]. For instance, monolayer single-crystalline MoS_2 has been controlled synthesized on SiO_2/Si substrates by CVD method and the device performances have been investigated by many groups [12–14]. Besides, Wang et al. reported a method capable of producing high crystalline rhomboid shaped MoS_2 microflakes with a controlled number of layers by further layer-by-layer sulfurization of as-synthesized MoO_2 microflakes [15]. For CVD-grown materials, substrate always has an essential influence on them, due to either lattice or thermal expansion coefficient mismatch induced strain or charge transfer effects across the contact interface. Moreover, the

* Corresponding author at: Institute of Super Microstructure and Ultrafast Process in Advanced Materials, College of Physics and Electronics, Central South University, 605 South Lushan Road, Changsha 410012, PR China.

E-mail address: bingchuyang@csu.edu.cn (B. Yang).

http://dx.doi.org/10.1016/j.ssc.2016.10.007
Received 22 March 2016; Received in revised form 4 August 2016; Accepted 9 October 2016
Available online 11 October 2016
0038-1098/

influence of underlying substrate on 2D materials could be significantly enhanced, attributed to their atomic thickness [16]. For instance, Raman and Photoluminescence (PL) emission of monolayer MoS_2 can be dramatically changed by the underlying substrates, due to charge transfer and strain effects [17,18]. Also, monolayer MoS_2 directly deposited on SiO_2/Si substrate exhibits different behaviors compared with transferred one, ascribed to thermal strain relief [17,19]. The rhomboid shaped MoS_2 is grown on MoO_2 crystal surface *via* sulfurization of its topmost layer, and triangle shaped MoS_2 is directly deposited on SiO_2/Si substrate, implying that two representative shaped MoS_2 have different underlying substrates [20]. Thus, it is necessary to systematically investigate physical properties evolutions of MoS_2 on SiO_2 and MoO_2 substrates.

In this contribution, we synthesized rhomboid shaped MoS_2/MoO_2 crystals through further sulfurization of MoO_2 crystals and equilateral triangle shaped MoS_2 single crystals through directly vapor phase deposited on SiO_2/Si substrate. The physical properties evolutions of synthesized two typical MoS_2 were systematically studied by various means. The X-ray photoemission spectroscopy results show that triangle shaped MoS_2 shows different core level spectra compared with rhomboid shaped MoS_2, indicating the dissimilar charge transfer effect with underlying substrates. In addition, a novel inhomogeneous electrostatic properties are observed at center and edges of triangle shaped MoS_2 while rhomboidal ones are identical across the entire surface investigated by Electrostatic Force Microscopy. We proposed the underlying mechanism that decoupling between MoS_2 edges with underlying SiO_2/Si substrate leads to inhomogeneous local doping and strain effects at interior and edges, which results in anomalous properties at edges.

2. Materials and methods

The experiments were carried out in a commercial CVD furnace (KJMTI Corporation, OTF-1200) with a 3 in.-diameter quartz tube and double heating zones in the length of 20 cm separated at border to border distance of 5 cm, as displayed in Fig. 1a. The growth temperature and carrier gas flow rate were controlled with a proportion integration differentiation (PID) temperature controller and a mass flow controller, respectively. A quartz boat loaded MoO_3 powders (4N purity, Aladdin) was placed at the 2nd heating zone while another loaded sulfur powders (5N purity, Aladdin) was placed at the center of the 1st heating zone of the furnace and at ~15 cm away at the upstream side. The sulfur weights for samples 1, 2 and 3 are 400, 500 and 600 mg, respectively, which is the unique variable since the MoO_3 weights (30 mg) for three samples are fixed. A third quartz boat with clean SiO_2 (300 nm thick)/Si substrate in 1×1 cm^2 was placed in the 2nd heating zone at the downstream side. The SiO_2/Si substrates were initially cleaned in DI water, acetone and isopropanol, following 3 h bath in H_2SO_4/H_2O_2 (volume ratio: 3:1) and by 5 min air plasma spurting to remove the possible organic contaminations. Upon roughly pumping, nitrogen (N_2, 5N purity) gas flow was introduced to purge the quartz tube at 150 sccm (standard cubic centimeters per minute) for 20 min. Then, the 2nd heating zone was rapidly heated up to 800 °C at a constant heating rate of 20 °C/min and maintained for 20 min with a decreased N_2 gas flow of 100 sccm, as displayed in Fig. 1b. Sulfur powders were maintained at the temperature being melting point of ~120 °C during the reaction process, so that sulfur vapor could be slowly carried by N_2 gas flow to the reaction zone. The system was maintained at pressure of 1 kPa during the entire growth run. Subsequently, the furnace was switched off following the growth process for cooling down to room temperature undisturbedly with N_2 gas flow.

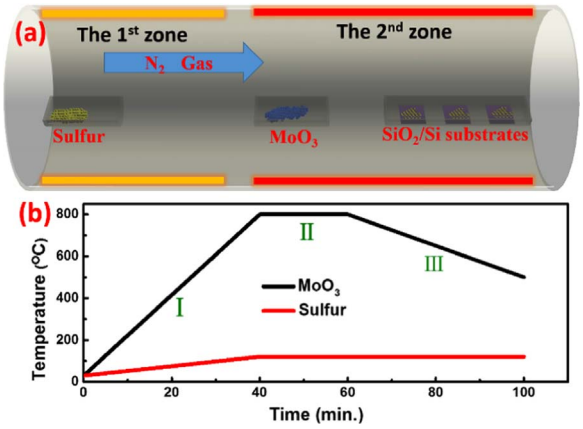

Fig. 1. (Color online) (a) A schematic diagram of the CVD system with double heating zones. The corresponding locations of sulfur, MoO_3 and SiO_2/Si substrates are marked in the CVD system. (b) Temperature programming process of MoO_3 and sulfur precursors.

The as-synthesized samples were systematically characterized by confocal Raman and photoluminescence techniques (WITec alpha 300R), X-Ray Photoemission Spectroscopy (XPS, thermo fisher ESCALAB 250xi), Atomic Force Microscopy and Electrostatic Force Microscopy (AFM/EFM, Agilent 5500). Raman and PL spectra/mapping were carried out under a 532.0 nm laser light and Si-based CCD detector at ambient conditions. The laser power was maintained below 1 mW to avoid local heating and oxidation to obtain a satisfactory signal-to-noise ratio while maintaining acceptable data acquisition duration and avoiding drift. The 520.0 cm^{-1} phonon mode from the silicon substrate was used for calibration of the Raman shift. The emitted signal was collected by a Zeiss 100× objective (N.A=0.9) and dispersed by a 1800 lines/mm grating for Raman measurements and a 600 lines/mm grating for PL measurements. The XPS investigations were performed using monochromatic Aluminium K_α X-Ray with light spot size of approximately 1 mm^2. The binding energy was calibrated by assigning the corresponding C 1 s peak at 284.5 eV. The AFM topography images and corresponding height profiles of three representative samples were characterized using AFM in tapping mode. The EFM investigations in amplitude modulation were also carried out at ambient conditions to explore local electronic properties of two typical MoS_2 surfaces. In our experiment, we used Pt/Ir-coated tip in tapping mode with a mechanical drive frequency of ~75 kHz for acquiring topography images and an Ac modulation of 0.2–0.3 V at 5–10 kHz for acquiring electrostatic images.

3. Results and discussion

Fig. 2a–c show the AFM topography images and corresponding height profiles (Insets) for three representative samples, respectively. Samples 1 and 2 are covered by rhomboid shaped crystals with size over 10 μm, which are assigned to MoO_2 or MoS_2/MoO_2 crystals. [15]. Sample 3 is covered by equilateral triangle shaped crystals, which are believed to be single-crystalline MoS_2 microflakes. Moreover, the inserted height profile (Fig. 2c) shows obvious plateaus with step height of ~1 nm, consistent with monolayer MoS_2.

We further performed XPS measurements to reveal the chemical composition of three representative samples. Fig. 2d–f display the XPS narrow scans of Mo 3d, S 2p and O 1s core level spectra for the three samples, respectively. The Mo 3d spectra for samples 1 and 2 exhibit two characteristic peaks centered at ~232.65 and ~229.54 eV below Fermi level, assigned to the doublet Mo $3d_{3/2}$ and $3d_{5/2}$ for Mo^{4+}[15,21]. The weak peak located at ~226.73 for sample 2 is assigned to S 2s [21]. The absence of such a peak for sample 1 suggests no detectable MoS_2. Moreover, the additional peaks centered at ~530.06 eV for samples 1 and 2 (Fig. 2f) are attributed to those from MoO_2. Thus, samples 1 and 2 can be assigned to MoO_2 and MoS_2/MoO_2, respectively, which is further confirmed by the S 2p core level spectra shown in Fig. 2e. On the basis of previous literatures, MoS_2 in sample 2 is believed to grow on outmost layer of rhomboidal MoO_2

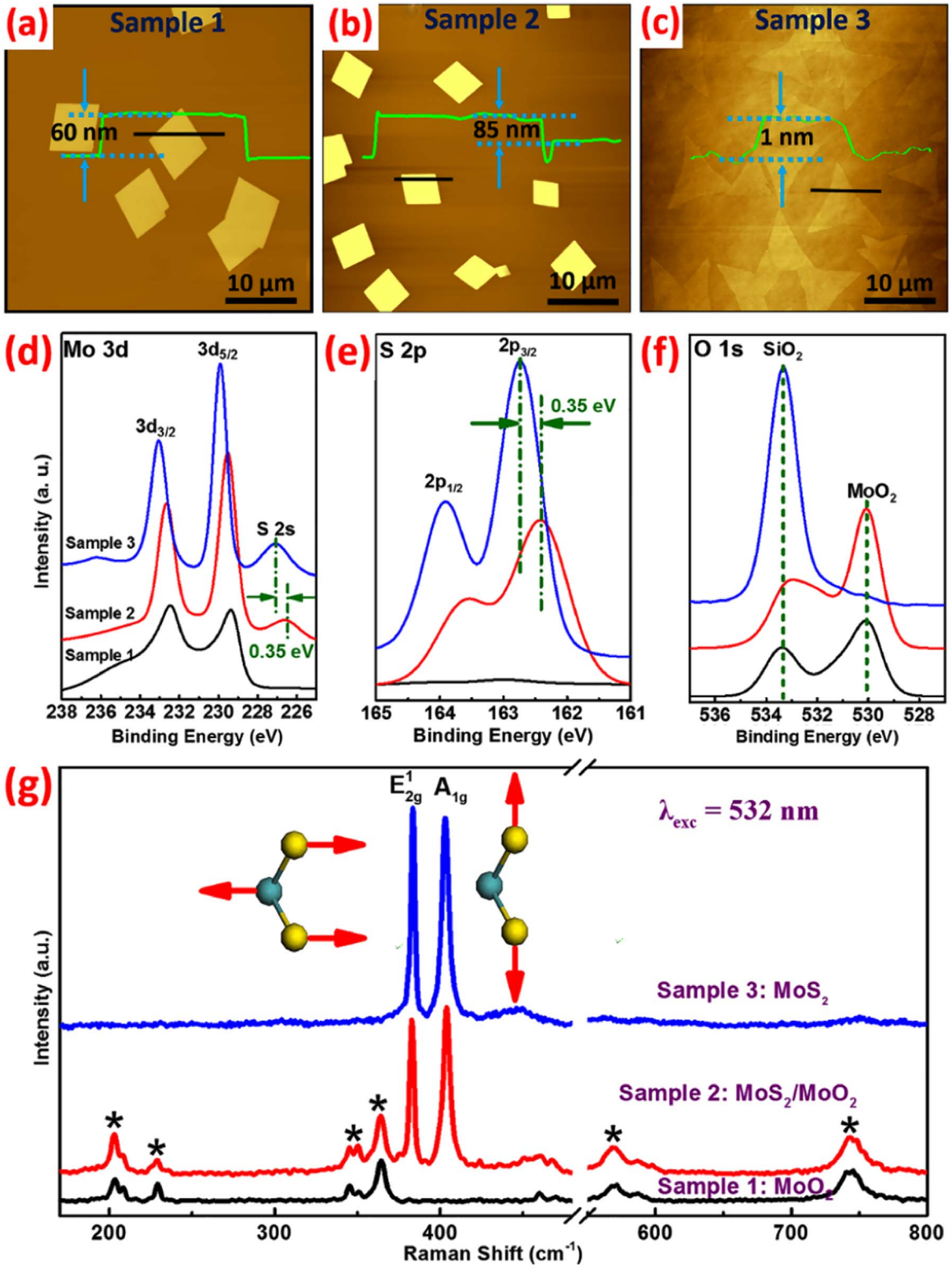

Fig. 2. (Color online) (a–c) The AFM topography images and corresponding height profiles scanned by green solid line (Insets) for three representative samples, respectively. (d-f) The corresponding Mo 3d, S 2p and O 1s core level spectra of XPS for three samples, respectively. (g) Raman spectra of MoO_2, MoS_2/MoO_2, and MoS_2 samples. Two characteristic modes E^1_{2g} and A_{1g} of MoS_2 are labeled and the corresponding cartoons are inserted. The peaks marked by asterisk are attributed to MoO_2.

islands through further layer-by-layer sulfurization rather than separate triangle shaped islands [15,22]. For sample 3, the obvious peaks for Mo and S elements are observed in Fig. 2d and e, respectively. Meanwhile, there is only one O 1s related peaks located at ~533.33 eV shown in Fig. 2f, which is attributed to the photoelectrons from the substrate (SiO_2), providing an unambiguous identification of pure MoS_2.

For sample 3, S related peaks shift toward higher binding energy by ~0.35 eV, suggesting a reduction of chemical state or a charge transfer effect. Given that a reduction of the -II chemical state of S is impossible, we interpret the cove level shift to charge transfer effects between MoS_2 surface and the underlying substrates. Firstly, we believe that it reflects

more electron donation to the MoS_2 from the underlying SiO_2 substrate, according to previous literatures [23–25]. Secondly, there is a band alignment in MoS_2/MoO_2, ascribed to different work functions between MoS_2 (4.5 eV) and MoO_2 (6.5 eV) [18,26]. Those results strongly indicate that the underlying substrates play a key role for electronic properties of MoS_2.

Fig. 2g presents the Raman spectra of three typical samples with an excitation wavelength of 532 nm. The peaks of sample 1 marked by asterisk are exclusively assigned to MoO_2 while two prominent characteristic peaks (E^1_{2g} and A_{1g}) for MoS_2 are absence, indicating that sample 1 is absolute MoO_2 [27,28]. For sample 2, all characteristic modes for MoO_2 as well as two prominent modes for MoS_2 (E^1_{2g} and A_{1g}) simultaneously appear, indicating coexistence of MoS_2 and MoO_2. The spectrum of sample 3 exhibits only two characteristic modes of MoS_2 without characteristic modes of MoO_2. Those results are fully consistent with XPS results and further support above-proposed three samples assignment. It has been well established that the intensity ratio of A_{1g} to E^1_{2g} modes can be altered by doping level since the A_{1g} mode is very sensitive to electron-phonon coupling [17,24]. In this regard, the intensity ratio of A_{1g} to E^1_{2g} modes exhibits differences for samples 2 and 3, indicating that sample 3 suffers from much serious n-type doping level. The behaviors arise from the substrate-induced doping effect, in excellent agreement with our XPS results.

In order to directly unveil the local electrical characteristics of MoS_2 on MoO_2 crystals and SiO_2/Si substrates, we performed the amplitude modulation single-pass EFM measurements. Generally, the conventional two-pass scan method inevitably introduces cross-talk between topography and electrostatic singal regardless of the lift distance set for the second scan [29]. Fig. 3a dipicts the schematic of our EFM measurements setup which is designed to simultaneously provid an efficient single-pass scan method to acquire the topography and EFM signals. The frequency corresponding to electrostatic force signal is chosen to be smaller than the cantilever mechanical oscillation frequency so that two signals do not interface with each other.

Fig. 3b–e present EFM topography and phase images of two representative MoS_2 single crystals, and the line-profiles extracted along green lines are inserted in their corresponding images. One can see that the electrostatic properties of rhomboidal MoS_2/MoO_2 domain are dependent on its morphology and identical across the entire surface owing to surface sulfurization of crystalline MoO_2 crystals [15]. Fig. 3b shows the AFM topography image and corresponding height profile, clearly exhibiting few triangle shaped single-crystalline MoS_2 with homogeneous structure between center and edges. However, the EFM phase image and corresponding profile clearly exhibit darker color at center and brighter color at edges, implying different electrostatic properties, in sharp contrast with rhomboidal ones. For our EFM measurements, repulsive force is presented in dark colar, which suggests that the interior regions suffer from larger n-doping level. On the basis of previous reports, there are at least two possible contributions to the changes in the electrostatic properties at MoS_2 edges and they will be discussed in detail later [17,18,30].

One contribution comes from the guest adsorbed contaminations which are often observed at the edge sites of MoS_2 crystals due to higher chemical reactivity [30]. It is mentioned that ambient contaminants are inevitably introduced during EFM scanning and the presence of these mobile dielectric molecules would affect the MoS_2 surface. Secondly, the underlying substrate has a strong influence on physical properties of micro-mechanical exfoliated MoS_2 microflakes investigated by Raman and PL technologies [17,18]. Hence, from our empirical observations, we suggest that the difference can be ascribed to inhomogeneous interactions between MoS_2 and SiO_2/Si substrate. Further experiments are required to support this postulate.

It has been shown that Raman spectroscopy can be used to estimate the interactions of monolayer MoS_2 with underlying substrate [31]. We first investigate the evolution of Raman spectra for MoS_2 at center and edges to elucidate the substrate effects, as displayed in Fig. 4a. The E^1_{2g} mode acquired from center and edges undergoes an red-shift compared with freestanding one, ascribed to an tensile strain induced by interactions with SiO_2/Si substrate [32,33]. Moreover, Raman spectroscopy shows an increase of the E^1_{2g} phonon frequency by 0.9 cm^{-1} at edges relative to center while A_{1g} mode does not shift acquired from edges compared to interior ones, demonstrating that single-crystalline MoS_2 edges sustain relative little strain than interior one. This can be well explained by that the strain at edges can be partially released (less strained) due to decoupling effects compared with interior one [33]. Similar result is also observed in WSe_2-MoS_2 lateral heterostructure, attributed to non-uniform strain distribution [34].

We further carried out PL spectroscopy/mapping to investigate influences of substrate on the optical properties of MoS_2 microflakes, as shown in Fig. 4b–d. Generally, PL spectrum of freestanding MoS_2

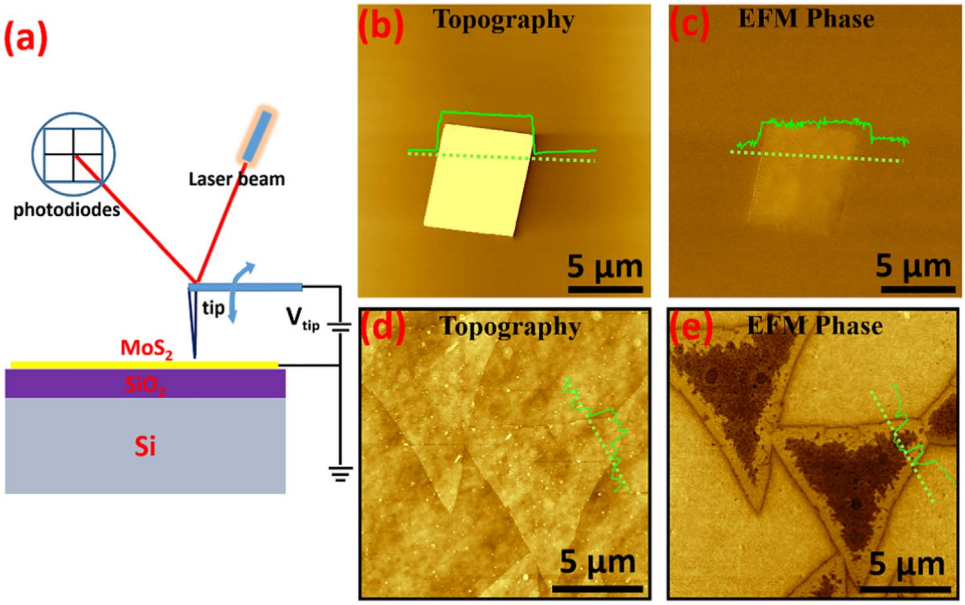

Fig. 3. (Color online) (a) Schematic of the EFM measurement setup. (b, c) The EFM topography and corresponding phase images of rhomboid shaped MoS_2/MoO_2 crystals, respectively. (d, e) The EFM topography and corresponding phase images of triangle shaped MoS_2 crystals, respectively. The corresponding line-profiles scanned by green lines are inserted in four images.

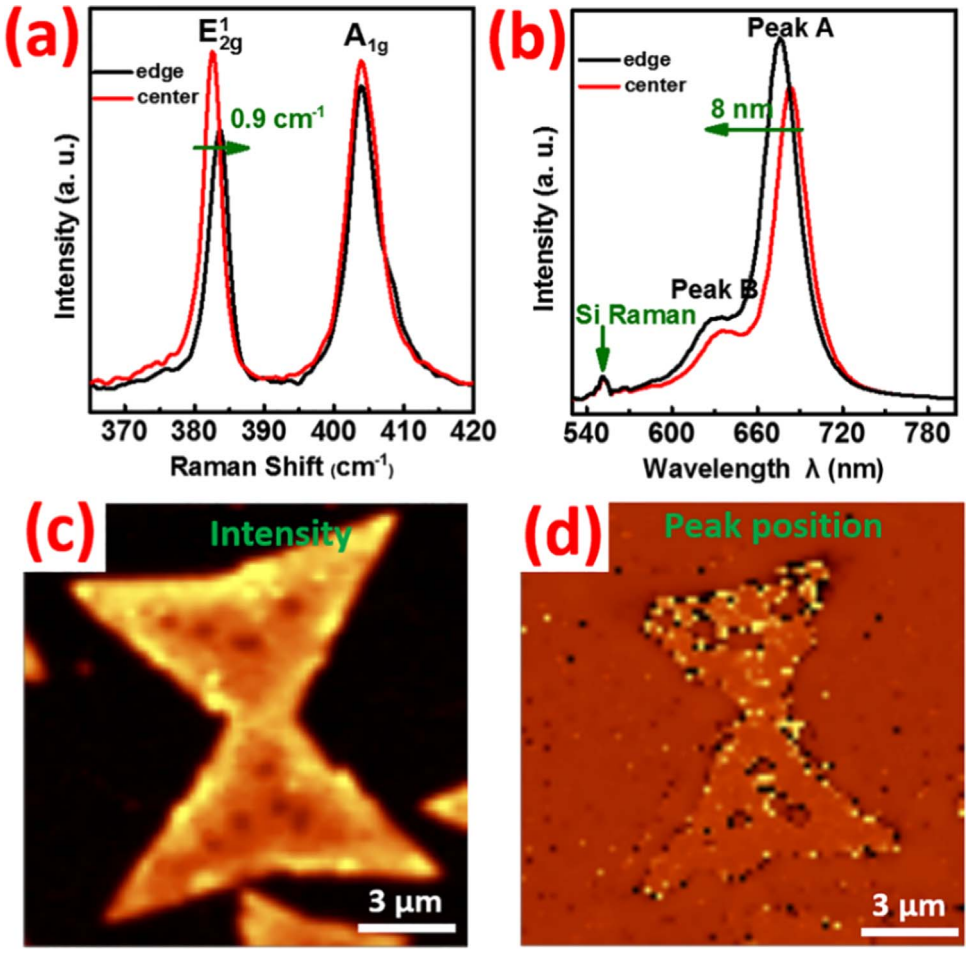

Fig. 4. (Color online) (a, b) Raman and PL spectra of triangle shaped MoS_2 acquired from center and edges, respectively. (c, d) The PL intensity and peak position mapping of peak A for MoS_2 on SiO_2/Si substrate.

presents two pronounced peaks located at ~670 nm (peak A) and ~630 nm (peak B), corresponding to the direct excitonic transition between the minimum of the conduction band and splitting valence bands at the k point [5,35]. Two characteristic PL peaks from interior are located at 638 nm (1.94 eV) and 683 nm (1.82 eV), while peaks from edges are centered at ~633 nm (1.96 eV) and ~675 nm (1.84 eV). Those results indicate that the PL spectra from interior and edges undergo a red-shift compared with freestanding ones, meanwhile, the spectrum from edges undergoes a blue-shift compared to interior ones. We interpret those shift to two sources and will discuss them in detail in the following.

Firstly, it is well established that doping effect can dramatically alter the PL emission by modulating the ratio between excitonic recombination and trion (charged exciton) recombination [24,36]. Our XPS results complemented with previous works demonstrate that CVD-grown MoS_2 is easy to be negatively doped by the underlying SiO_2 /Si substrate [24,25]. Moreover, the intensity ratio of A_{1g} to E^1_{2g} modes, which is in consistent with doping level, indicate that the n-type doping level at interior is higher than edge ones, ascribed to above-mentioned decoupling effect [17,31]. Therefore, we conclude that there is an inhomogeneous doping level between center and edges, which is responsible for the distinct PL emission. Moreover, the position mapping of peak A (Fig. 4d) shows two obvious color contrast between center and edges, demonstrating that the different doping level concluded from PL spectra is through the single crystal rather than some special points. We notice that the electrostatic behavior at edges is well consistent with PL peak position mapping, where the properties at edges are rather distinct from interior ones. Thus, it provides a further complementary proof of decoupling effect at edges induced distinct doping level, which leads to anomalous electrostatic and photoluminescence properties at MoS_2 edges.

Secondly, Raman results complemented with previous literature suggest that a tensile thermal strain is resulted in triangle shaped MoS_2 crystals, due to thermal expansion coefficient mismatch [33]. In addition, the tensile strain at edges is smaller than interior one, attributed to partially strain relief. As for the fact that the optical bandgap of monolayer MoS_2 decreases at a rate of ~45 meV/% tensile strain, the optical bandgap at edges would be larger than interior one, resulting in blue-shift of PL peaks [37].

4. Conclusions

In conclusion, the rhomboid shaped MoS_2 on MoO_2 crystals and triangle shaped MoS_2 on SiO_2/Si substrate are successfully prepared by CVD method. We found that the triangle shaped MoS_2 shows apparent charge transfer with the underlying SiO_2 substrate compared to rhomboidal one. In addition, the edges of triangle shaped monolayer MoS_2 exhibit extraordinary electrostatic signals and PL emission compared with interior ones. The proposed underlying mechanism is that the inhomogeneous local interactions between MoS_2 and SiO_2 substrate induce different doping and strain effects, which is responsible for evolution of physical properties between MoS_2 edges and interior. These findings deepen the understanding of physical properties evolution and the roles of substrate on CVD-grown monolayer MoS_2 being local doping and strain effects.

Acknowledgement

We acknowledge the financial support from the National Natural Science Foundation of China (Grants no. 11304398, 11334014, 51173205).

References

[1] A.K. Geim, Science 324 (2009) 1530–1534.
[2] M. Chhowalla, H.S. Shin, G. Eda, L.J. Li, K.P. Loh, H. Zhang, Nat. Chem. 5 (2013) 263–275.
[3] Y.C. Lin, D.O. Dumcenco, Y.S. Huang, K. Suenaga, Nat. Nanotechnol. 9 (2014) 391–396.
[4] J.M. Lu, O. Zheliuk, I. Leermakers, N.F.Q. Yuan, U. Zeitler, K.T. Law, J.T. Ye, Science 350 (2015) 1353–1357.
[5] K.F. Mak, C. Lee, J. Hone, J. Shan, T.F. Heinz, Phys. Rev. Lett. 105 (2010) 136805.
[6] B. Radisavljevic, A. Radenovic, J. Brivio, V. Giacometti, A. Kis, Nat. Nanotechnol. 6 (2011) 147–150.
[7] H. Wang, L. Yu, Y.H. Lee, Y. Shi, A. Hsu, M.L. Chin, L.J. Li, M. Dubey, J. Kong, T. Palacios, Nano Lett. 12 (2012) 4674–4680.
[8] H.S. Lee, S.W. Min, Y.G. Chang, M.K. Park, T. Nam, H. Kim, J.H. Kim, S. Ryu, S. Im, Nano Lett. 12 (2012) 3695–3700.
[9] X. Li, W. Cai, J. An, S. Kim, J. Nah, D. Yang, R. Piner, A. Velamakanni, I. Jung, E. Tutuc, S.K. Banerjee, L. Colombo, R.S. Ruoff, Science 324 (2009) 1312–1314.
[10] H. Nguyen, C.-F. Huang, W. Luo, G. Xia, Z. Chen, Z. Li, C. Raymond, D. Doyle, F. Zhao, Mater. Lett. 168 (2016) 1–4.
[11] D. MacMahon, A. Brothers, K. Florent, S. Kurinec, Mater. Lett. 161 (2015) 96–99.
[12] Y.H. Lee, X.Q. Zhang, W. Zhang, M.T. Chang, C.T. Lin, K.D. Chang, Y.C. Yu, J.T. Wang, C.S. Chang, L.J. Li, T.W. Lin, Adv. Mater. 24 (2012) 2320–2325.
[13] Q. Ji, Y. Zhang, T. Gao, Y. Zhang, D. Ma, M. Liu, Y. Chen, X. Qiao, P.H. Tan, M. Kan, J. Feng, Q. Sun, Z. Liu, Nano Lett. 13 (2013) 3870–3877.
[14] S. Najmaei, Z. Liu, W. Zhou, X. Zou, G. Shi, S. Lei, B.I. Yakobson, J.C. Idrobo, P.M. Ajayan, J. Lou, Nat. Mater. 12 (2013) 754–759.
[15] X. Wang, H. Feng, Y. Wu, L. Jiao, J. Am. Chem. Soc. 135 (2013) 5304–5307.
[16] A.J. Bradley, M.M. Ugeda, F.H. da Jornada, D.Y. Qiu, W. Ruan, Y. Zhang, S. Wickenburg, A. Riss, J. Lu, S.K. Mo, Z. Hussain, Z.X. Shen, S.G. Louie, M.F. Crommie, Nano Lett. 15 (2015) 2594–2599.
[17] M. Buscema, G.A. Steele, H.S.J. van der Zant, A. Castellanos-Gomez, Nano Res. 7 (2015) 561–571.
[18] Y. Li, Z. Qi, M. Liu, Y. Wang, X. Cheng, G. Zhang, L. Sheng, Nanoscale 6 (2014) 15248–15254.
[19] Y. Kang, Y. Gong, Z. Hu, Z. Li, Z. Qiu, X. Zhu, P.M. Ajayan, Z. Fang, Nanoscale 7 (2015) 4482–4488.
[20] B. Hu, L.Q. Mai, W. Chen, F. Yang, ACS Nano 3 (2009) 478–482.
[21] A.S. George, Z. Mutlu, R. Ionescu, R.J. Wu, J.S. Jeong, H.H. Bay, Y. Chai, K.A. Mkhoyan, M. Ozkan, C.S. Ozkan, Adv. Funct. Mater. 24 (2014) 7461–7466.
[22] Q. Ji, Y. Zhang, Y. Zhang, Z. Liu, Chem. Soc. Rev. 44 (2015) 2587–2602.
[23] D. Sercombe, S. Schwarz, O. Del Pozo-Zamudio, F. Liu, B.J. Robinson, E.A. Chekhovich, I.I. Tartakovskii, O. Kolosov, A.I. Tartakovskii, Sci. Rep. 3 (2013) 3489.
[24] S.S. Wang, X.C. Wang, J.H. Warner, ACS Nano 9 (2015) 5246–5254.
[25] C.P. Lu, G. Li, J. Mao, L.M. Wang, E.Y. Andrei, Nano Lett. 14 (2014) 4628–4633.
[26] Y. Liang, C. Tracy, E. Weisbrod, P. Fejes, N.D. Theodore, Appl. Phys. Lett. 88 (2006) 081901.
[27] H. Li, Q. Zhang, C.C.R. Yap, B.K. Tay, T.H.T. Edwin, A. Olivier, D. Baillargeat, Adv. Funct. Mater. 22 (2012) 1385–1390.
[28] M. Dieterle, G. Mestl, Phys. Chem. Chem. Phys. 4 (2002) 822–826.
[29] S.Xa.M.F. Arnsdorf, Proc. Natl. Acad. Sci. USA 92 (1995) 10384–10388.
[30] Y.L. Huang, Y. Chen, W. Zhang, S.Y. Quek, C.H. Chen, L.J. Li, W.T. Hsu, W.H. Chang, Y.J. Zheng, W. Chen, A.T. Wee, Nat. Commun. 6 (2015) 6298.
[31] B.J. Robinson, C.E. Giusca, Y.T. Gonzalez, N.D. Kay, O. Kazakova, O.V. Kolosov, 2D Mater. 2 (2015) 015005.
[32] N. Scheuschner, O. Ochedowski, A.-M. Kaulitz, R. Gillen, M. Schleberger, J. Maultzsch, Phys. Rev. B 89 (2014) 125406.
[33] Z. Liu, M. Amani, S. Najmaei, Q. Xu, X. Zou, W. Zhou, T. Yu, C. Qiu, A.G. Birdwell, F.J. Crowne, R. Vajtai, B.I. Yakobson, Z. Xia, M. Dubey, P.M. Ajayan, J. Lou, Nat. Commun. 5 (2014) 5246.
[34] M.Y. Li, Y.M. Shi, C.C. Cheng, L.S. Lu, Y.C. Lin, H.L. Tang, M.L. Tsai, C.W. Chu, K.H. Wei, J.H. He, W.H. Chang, K. Suenaga, L.J. Li, Science 349 (2015) 524–528.
[35] A. Splendiani, L. Sun, Y. Zhang, T. Li, J. Kim, C.Y. Chim, G. Galli, F. Wang, Nano Lett. 10 (2010) 1271–1275.
[36] S. Tongay, J. Suh, C. Ataca, W. Fan, A. Luce, J.S. Kang, J. Liu, C. Ko, R. Raghunathanan, J. Zhou, F. Ogletree, J. Li, J.C. Grossman, J. Wu, Sci. Rep. 3 (2013) 2657.
[37] H.J. Conley, B. Wang, J.I. Ziegler, R.F. Haglund Jr., S.T. Pantelides, K.I. Bolotin, Nano Lett. 13 (2013) 3626–3630.